



## Thermal comfort performance prediction method using sports center layout images in several cold cities based on CNN

Ao Xu <sup>a,b</sup>, Yu Dong <sup>a,b</sup>, Yutong Sun <sup>a,b</sup>, Haoqi Duan <sup>a,b</sup>, Ruinan Zhang <sup>a,b,\*</sup>

<sup>a</sup> School of Architecture, Harbin Institute of Technology, Harbin, 150001, China

<sup>b</sup> Key Laboratory of Cold Region Urban and Rural Human Settlement Environment Science and Technology, Ministry of Industry and Information Technology, Harbin, 150001, China



### ARTICLE INFO

#### Keywords:

Convolutional neural network  
Sports center layout  
Outdoor thermal comfort  
Urban form index  
Urban microclimate

### ABSTRACT

Sports centers are core spaces for urban sports and fitness, and reasonable layout of large public buildings can alleviate urban climate issues. But the adverse effects of planning and layout and surrounding urban microclimate on the thermal comfort of outdoor activity space are rarely considered. In this study, an EnergyPlus and Openfoam collaborative computing platform was constructed to calculate the universal thermal climate index of the outdoor space of sports center. By comparing the simulation results of sports centers in three severely cold cities, improving the wind environment of the site's microclimate was found to be key in improving thermal comfort, and the hours of overall site thermal comfort increased mainly in spring and autumn. In this paper, a design method combining numerical simulations and a convolutional neural network was proposed, which can effectively predict the thermal comfort performance of affected sites. The application of this prediction method to the design of the Yingkou Sports Center increased the hours of overall site thermal comfort by 15.01% compared with the original scheme. Synthesizing the results and methods of this study can provide an effective reference and analysis tool for the overall environmental performance of urban areas.

### 1. Introduction

Global urbanization is accelerating and over half of the world's population lives in urban areas [1]. Climate change, the urban heat island effect, energy consumption, and pollution emissions caused by population growth and land expansion in urban areas have attracted significant attention [2]. These phenomena are particularly prominent in China, which is undergoing rapid urbanization and is expected to reach an urbanization rate of 65.5% by 2025 [3]. In the context of sustainability, energy conservation, and emission reduction, issues such as the microclimate, decreasing carbon emissions, health, and thermal comfort in urban built environments have become popular topics [4]. Outdoor thermal comfort is a key factor affecting outdoor activities, physiological health, building energy consumption, and urban livability [5–7]. Many studies have confirmed that long-term exposure to non-thermal comfort zones can cause serious health problems, decrease human motor function, and increase the risk of sports injuries [8]. Li

et al. systematically reviewed the research related to thermal comfort in China and posited that the influences of block shape, landscape, high-rise buildings, and pavement configuration on thermal comfort in microclimates have been sufficiently studied, with the research scope mainly focusing on the building and block scales [9]. Therefore, recent studies on microclimates and thermal comfort have gradually progressed from a smaller scale to a larger urban scale [3,10–12].

With improvements in material and lifestyle standards and the increasing threat of potentially infectious diseases to public health worldwide, a global consensus has been reached on the importance of national fitness and healthy built environments. Sports architecture systems have gradually improved, and the amount of related research on sports building environments has increased. Owing to the orientation of urban development policies and the development of intensive design concepts, sports centers have become a mainstream form of construction for large sports facilities in China in recent years. As a common building type in cities and regions, sports centers are important supporters of

**Abbreviations:** ALI, aggregation of layouts index; CFD, computational fluid dynamics; CNN, convolutional neural network; ESI, effective sunshine hours index; MRT, mean radiation temperature; MSE, mean square error; RANS, Reynolds-mean Navier–Stokes; R2, coefficient of determination; RMSE, root mean square error; UTCI, universal thermal climate index; WFI, windward area of the building after the annual wind frequency correction.

\* Corresponding author. School of Architecture, Harbin Institute of Technology, Harbin, 150001, China.

E-mail address: [17b334006@stu.hit.edu.cn](mailto:17b334006@stu.hit.edu.cn) (R. Zhang).

<https://doi.org/10.1016/j.buildenv.2023.110917>

Received 8 August 2023; Received in revised form 7 October 2023; Accepted 9 October 2023

Available online 10 October 2023

0360-1323/© 2023 Elsevier Ltd. All rights reserved.

healthy cities and lives. Sports centers usually occupy a large amount of land and have a large volume, convenient transportation links, and diversified functions, resulting in a strong urban agglomeration effect. With the upgrade of event scales and sports demand, outdoor venues are following a trend of free opening and organic integration with cities. The infiltration of parks and sports venues has resulted in the gradual expansion of their site scales, which have exceeded the standard block scale.

According to the China Design Code for Sports Buildings [13], sports centers are usually one stadium and two or more gymnasiums. Sports centers are built based on city size, population, the economy, etc. Their scale can be summarized as investment or building scale (area and seat scales, respectively). The scale of a building depends mainly on the functional positioning of the center, the needs of the city, and the investment scale. At present, small- and medium-sized cities in China mainly contain one stadium and two gymnasium-type sports centers, which are built in provincial capitals or cities with better economic development. Based on the division of climate zones in the China Unified Standards for Civil Building Design [14], we reviewed the layouts and scales of sports centers in three provinces of China with severely cold climate zones (Heilongjiang, Jilin, and Liaoning), as shown in Fig. 1.

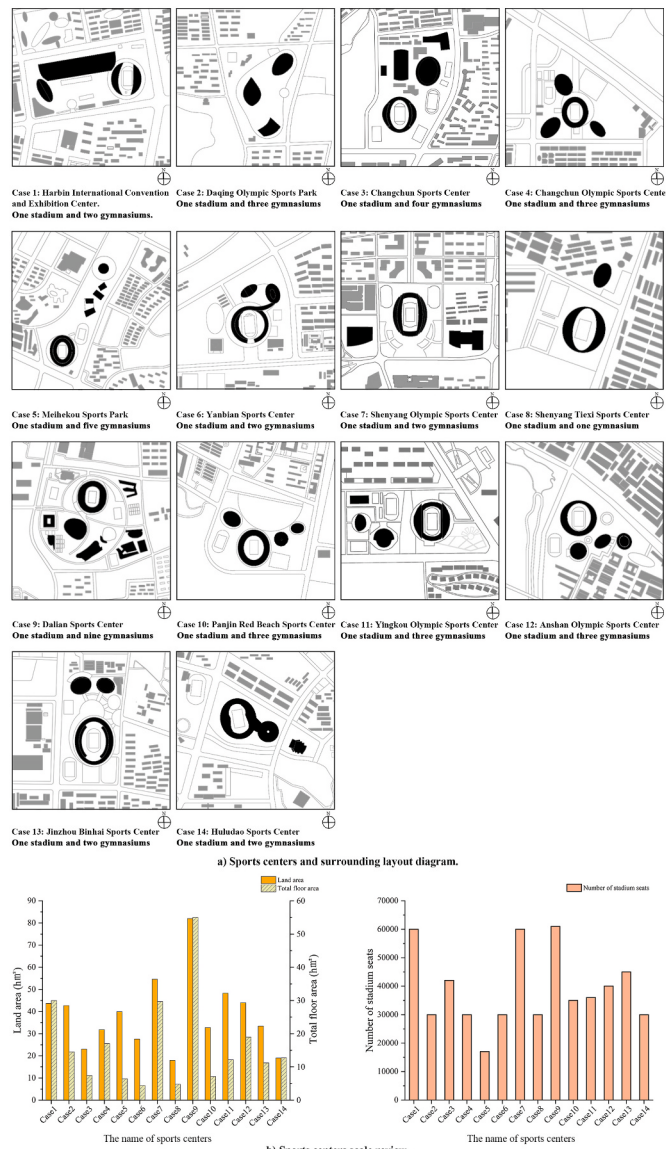


Fig. 1. Survey of sports centers in severe cold region of China.

According to the review, we selected three representative sports centers to further explore the influence of sports center venue layout on the urban microclimate and site thermal comfort.

The characteristics of sports centers must coordinate and integrate with urban development. Starting from the overall spatial environment of the city, this study explored the relationship between the layout of large-scale sports buildings and the city, which is helpful for improving the effective utilization of sports center sites. More importantly, architectural layout planning and design have strong regional requirements, particularly for outdoor venues. The urban form index and scientific design method for sports center planning proposed in this study can provide theoretical support and a reference for future sports center construction.

## 2. Literature review

### 2.1. Thermal comfort of sports buildings

With the maturation of building performance simulations and concerns regarding sustainable and healthy built environments, research on the thermal comfort performance optimization design of sports buildings is gradually increasing. Huang et al. proposed the optimization of naturally ventilated gymnasiums. Through a combination of architectural form optimization, simulation, and orthogonal test methods, the influence of sports architectural forms on indoor thermal comfort has been explored [15], as well as the influence of sports architectural interface forms on the thermal comfort of gymnasiums [16]. Yefei et al. evaluated the indoor thermal environment of a membrane-structured gymnasium using a combination of field testing and questionnaire surveys to propose improvement measures [17]. Scholars have also conducted relevant research on thermal comfort in stadiums. Losi et al. analyzed the thermal comfort of stadium users in hot and humid climates using computational fluid dynamics (CFD) simulations based on an air-conditioning system [18]. Saud et al. conducted a comparative study on the applicability of seven thermal comfort indices to stadiums [19]. Ruinan et al. conducted energy and CFD simulations, combined artificial neural networks and genetic algorithms for optimization, and proposed an effective form optimization method to improve the thermal comfort performance of semi-outdoor stadiums [20]. Although the thermal comfort performance of sports buildings has received extensive attention, most studies focused on individual stadiums and/or gymnasiums. Related research based on a complex of multiple venues in sports centers remains insufficient. Kim and Hyon-U focused on the flow field formed around large stadiums; however, they did not conduct research on thermal comfort [21]. Outdoor thermal comfort has been explored for high-density blocks, residential areas, squares, and other research objects [22–24]. Although outdoor thermal comfort has been thoroughly studied in high-density neighborhoods, residential areas, squares, and parks, the methods and evaluation criteria proposed in these studies need to be further explored and verified for sports centers.

### 2.2. Influence of urban form index on thermal comfort

In previous studies, the methods to determine the impact of urban form on urban microclimates were divided into three main categories: one used urban morphology parameters to study real cases [25–27]; Xingzhao Zhang and Jiawei Yao et al. selected eight morphological indicators to evaluate the outdoor environments of worker villages in eastern China using machine learning [28]. He et al. selected 12 primary schools in highly urbanized areas as research objects. Based on field measurements and ENVI-met simulations, they concluded that the building density, floor area ratio, greening rate, and sky landscape factors were important urban form parameters affecting the microclimate around primary schools [29]. Notably, the degree of importance of the urban form index may vary at different urban scales. Galal et al. explored the influence of urban forms on outdoor thermal comfort and

found that different urban form indices had different impacts on thermal comfort at the block and street scales [30]. The second category of methods investigates typical architectural forms or extracts classic design urban form strategies to explore limited cases [31]; Eslamirad et al. defined 11 typical building forms and shapes according to Tallinn urban planning and evaluated the outdoor thermal and wind comfort of the northern urban environment using machine learning models [32]. Sun et al. proposed three combinations of boxes with different lengths, widths, and directions to represent buildings and suggested an outdoor space design for kindergartens in Tianjin and Shanghai [33]. The third category combines the first and second methods [34]. Deng et al. selected three different prototypes, namely freestanding, scattered, and enclosed, as representatives of typical urban forms in the central urban area of Nanjing and compared and analyzed the impact of urban morphological characteristics on the outdoor thermal environment [35]. Generally, studies using urban morphological parameters are mostly performed at the block scale or larger, whereas the sampling of typical architectural layout forms is primarily based on the external environment at the block or building scale. In addition, urban morphological parameters have strong universality, and some parameters integrate urban planning indicators, such as floor area ratio, floor area, and sky view factor, which do not affect building geometry and leave creative space for architects. Typical building forms are relatively limited because objects have relatively regular forms with few changes, such as board houses, office buildings, and regular blocks.

In summary, as representative large urban public buildings, sports facilities often simultaneously carry the functions of providing regional vitality, affecting the urban image, and supporting cultural traditions; therefore, using an abstract typical form is not appropriate and has weak universality. In addition, owing to the characteristics of sports venue layouts, commonly used urban form indices, such as sky factor, building height, and building density, are not suitable for evaluating thermal comfort. Therefore, it is necessary to propose more effective urban form indicators for the layout of sports centers.

### 2.3. Main innovations

- From the urban microclimate perspective, this study aims to explore the mutual influence between the layout of a sports center and the thermal climate of the surrounding city through three cases with similar scales but different surroundings.
- To improve the overall thermal comfort of the site, three types of urban form indices that control the planning and layout of the sports center are proposed. The effects of different layouts on the thermal comfort during different periods were also analyzed.
- This study proposes a layout design method for sports centers in severely cold areas by training a convolutional neural network (CNN) that provides guidance for early site layout design.
- A surrogate model was used to quickly predict the thermal comfort performance and the influence of urban form indices on the outdoor thermal comfort of sports centers under a certain urban microclimate.

## 3. Method

This study is divided into two main parts. In the first part, three real cases from the Changchun, Shenyang Olympic, and Yingkou Olympic Sports Centers were selected through EnergyPlus, CFD simulations, and field measurements. The universal thermal climate index (UTCI) was used as the thermal comfort index to explore the scope and mechanism of mutual influence between urban form and sports center layout from the urban microclimate perspective. In the second part, the Yingkou Olympic Sports Center was used as an example to explore the influence of the layout of the sports center on the microclimate at the site. For the Yingkou Olympic Sports Center layouts generated, the location of the central point of the building was controlled to ensure that the distance

between any two central points was greater than 1.2 times the sum of the radii of the two buildings, and the boundary of each building was also controlled to be over 20 m from the outer boundary of the site. Based on these rules, 400 layout schemes were randomly generated.

The CNN is used to effectively improve the thermal comfort performance evaluation efficiency of outdoor venues with different layouts of sports centers, and the regression analysis and advantage range analysis are carried out through the urban form index and the thermal comfort performance of the venues. To explore the relationship between the urban form index and the thermal comfort performance of sports centers.

In conclusion, this paper establishes a workflow based on CNN to predict the thermal comfort performance of outdoor venues in the layout of sports centers, and explores the specific influence ways and reasons for the influence of urban microclimate between sports centers and surrounding urban environments through three real cases. The workflow can effectively improve the layout optimization efficiency of large-scale public buildings such as large-scale sports centers. The proposed urban form index can provide an effective reference and analysis tool for the improvement of the environmental performance of urban regions. Fig. 2 illustrates the framework of this study.

### 3.1. Case study

Fourteen typical sports centers in Heilongjiang, Jilin, and Liaoning provinces in the severely cold climate zone of China were reviewed. The study area is located in northeastern China, with four distinct seasons, short and cool summers, long and cold winters, abundant sunshine, large solar radiation, and strong wind speeds. The three cases selected in this study, namely Changchun, Shenyang Olympic, and Yingkou Olympic Sports Centers, are in line with the standard definitions of sports centers. The three cases are slightly different, and they are all typical first-class comprehensive sports centers in China. In addition, these three cases were selected because their surrounding environments included diverse urban form characteristics and types, such as low-rise residential areas, high-rise residential areas, urban parks, high-rise commercial areas, universities, and other urban form characteristics. The scope of this study is illustrated in Fig. 3(a). Owing to the slightly different occupation scales, they were set within the rectangular range of 1200 m\*1500 m, 1500 m\*1000 m, and 1500 m\*1300 m, respectively. We consider the real surrounding urban form and terrain influence in this case. In this study, three indices were selected to parametrically control the venue layout. The parameterized model and simulation were integrated in the Rhino-Grasshopper platform, and the model accuracy is in meters (m) with an absolute tolerance of 0.01. Fig. 3(b) provides a schematic diagram of urban form indices' definitions.

Three layout parameters were extracted to explore the influence of the sports centers layout on the thermal comfort quality of the activity area. In view of the evident influence of wind speed and mean radiation temperature (MRT) on thermal comfort, the average effective sunshine hours index (ESI) at the site and the windward area of the building after annual wind frequency correction (WFI) were extracted as parameters. Through a multi-case investigation and simulation, the results revealed that the convergence degree of the building layout affected the wind speed distribution and the degree of overlap of building shadows at the site to a certain extent. Therefore, the degree of aggregation of layouts index (ALI) was considered the third geometrical parameter in this study.

The ESI, WFI and ALI are calculated with the below formulas.

$$ESI = \frac{\sum_{i=1}^n h_i}{n} \quad (1)$$

where  $n$  represents the number of test points, and  $h_i$  represents the number of total daylight hours per test point throughout the year. In this

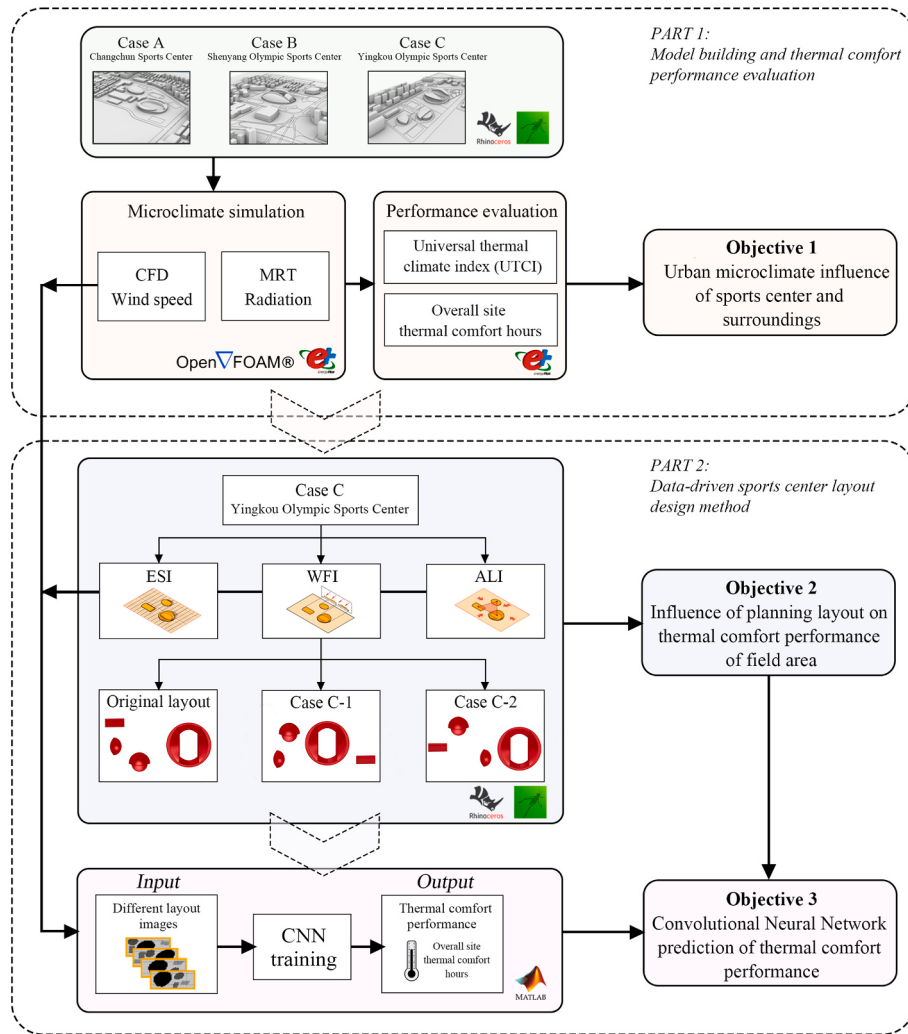


Fig. 2. Study framework.

study, 5200 test points were evenly distributed throughout the site, indicating that  $n = 5200$ .

$$WFI = \sum_{i=1}^n S_i \times f_i = S_i \times \frac{e_i}{H} \quad (2)$$

where  $n$  represents the number of wind directions throughout the year,  $S_i$  represents the windward area of the buildings in each wind direction, and  $f_i$  represents the frequency of each wind direction during the 4380 test hours throughout the year. In this study, the test period was set from 6:00 a.m. to 5:00 p.m. every day during the spring, summer, autumn and winter. Therefore,  $H$  represents the number of test hours ( $H = 4380$ ) and  $e_i$  represents the number of hours in which each wind direction was present during the test period. Given the weather station data, 16 wind directions were recorded, so  $n$  was set to 16 in this formula.

$$ALI = \frac{A_S}{A_T} \quad (3)$$

where  $A_S$  represents the area enclosed by the central points of the buildings and  $A_T$  represents the total test area of the site.

### 3.2. CFD-MRT-UTCI calculation

In this study, air velocity was simulated using OpenFoam, and MRT was calculated using EnergyPlus. UTCI, selected as the thermal comfort index, was computed using the UTCI calculator program. The hours of

the overall site thermal comfort were calculated using Rhino-Grasshopper. The formulae for each part are given below.

For the CFD simulation, we selected the Reynolds-mean Navier-Stokes (RANS) equation model simulation on the OpenFoam platform. Existing research has applied RANS simulations to study the influence of building geometry, planning layout, and urban microclimate on external thermal comfort [36–38]. In the chtMultiRegionSimpleFoam OpenFOAM solver, the buoyancy, turbulent fluid flow, and heat conduction transfer between the exterior surfaces and fluid regions were simulated. The formula is as follows:

$$\frac{\partial h}{\partial t} + \mu \cdot \nabla(\rho h) + \rho \mu \cdot \nabla \left( \frac{1}{2} \mu \cdot \mu \right) = -\nabla \cdot q + S_H \quad (4)$$

where  $\rho$  represents the fluid density,  $\mu$  represents the fluid velocity,  $q$  represents the thermal flux, and  $S_H$  is a source term, which is used to include the solar radiation [39].

In urban CFD simulation, box-shaped domain and cylindrical domain shape can be used as the computational domain. In this study, in order to simulate the operation period of the sports centers throughout the year, the use of box-shaped domain has a defect in the study of wind conditions, and the grid needs to be reset whenever the wind direction changes. The cylindrical domain can reduce the complexity of the simulation grid operation and reduce the time consumption [40,41]. Therefore, the cylindrical domain is chosen to study in this paper. Referring to the studied wind tunnel size and grid-independence

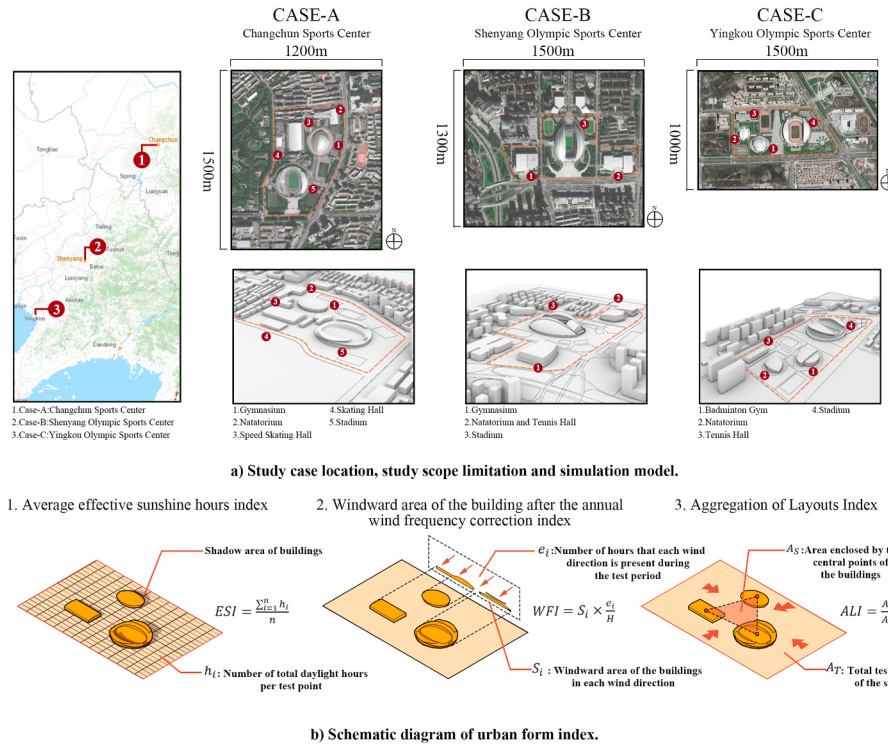


Fig. 3. Case definition and urban form index diagram.

analysis table (Table 1 in the Supplementary Materials), the CFD simulation settings are listed in Table 1. The simulated grid settings are shown in Fig. 4. In addition, this study considered thermal comfort throughout the year in different layouts, rather than for a few hours or days, over a specific period of time, and steady-state simulations were used to reduce the required amount of computation.

The most popular devices for MRT evaluation are convenient and accessible global thermometers. MRT validation requires measuring the black-globe temperature and air velocity at the height of the measurement [42]. EnergyPlus is a common and convenient tool used for simulating MRT [43]. The MRT at each measurement point in the simulation primarily depends on the surrounding temperature. The angle factor MRT algorithm based on the Rhino-Grasshopper platform can predict the thermal comfort of a specific location more accurately than other methods. The equation is:

$$T_{mrt} = \frac{\sum \varepsilon_i F_i (T_i)^4}{\sum \varepsilon_i F_i} \quad (5)$$

**Table 1**  
Simulation settings.

Simulation	Simulation Tools	Constant Items	Case A Values	Case B Values	Case C Values
CFD	Openfoam	Location	43°90'N 125°21'E	41°73'N 123°45'E	40°67'N 122°17'E
		Temperature range	-27.3–33 °C	-23.4–34.1 °C	-26 - 33 °C
		Wind speed range	0–17 m/s	0–17 m/s	0–20 m/s
		Wind direction	0°, 45°, 90°, 135°, 180°, 225°, 270°, 315°		
		Boundary type	Cylindrical domain		
		Boundary Inner rectangle	2400 m	2600 m	2000 m
		Boundary Outer radius	8000 m	9000 m	7000 m
		Boundary height	250 m		
		Mesh size	1,252,917	2,398,411	1,703,004
		Mesh type	OpenFOAM's blockMesh and snappyHexMesh		
MRT	EnergyPlus	CFD Turbulence model	RealizableKE		
		Pressure model	SIMPLE (Semi Implicit Method for Pressure Linked Equations)		
		Concrete (emissivity of the surface)	0.95		
		Asphalt (emissivity of the surface)	0.92		
		Lawn (emissivity of the surface)	0.78		

where  $T_{mrt}$  represents MRT,  $\varepsilon_i$  represents the emissivity of the surface,  $F_i$  is the angle factor between the test point and the surrounding surface,  $T_i$  is the surface temperature in the simulation, and  $i$  is the surrounding surface number. The MRT simulation settings are listed in Table 1.

UTCI is generalized for efficient assessment procedures for thermal comfort in various fields [44,45]. UTCI adopts the Fiala model, which is an accessible model of human thermoregulation with extensive validation. This equation can be roughly described as follows [46]:

$$\begin{aligned} UTCI = & \int (T_a; T_{mrt}; v_{10}; RH; Met; Clo) = T_a \\ & + Offset(T_a; T_{mrt}; v_{10}; RH; Met; Clo) \end{aligned} \quad (6)$$

where  $T_a$  is the air temperature,  $T_{mrt}$  is the MRT,  $v_{10}$  is the air velocity at a height of 10 m,  $RH$  is the relative humidity,  $Met$  is the metabolic rate, and  $Clo$  is clothing insulation value. To obtain accurate simulation results, we set the physiological metabolism as 9.5 (running at 9 mph) and the clothing index as 0.5 in the spring and autumn, 0.3 in the summer,

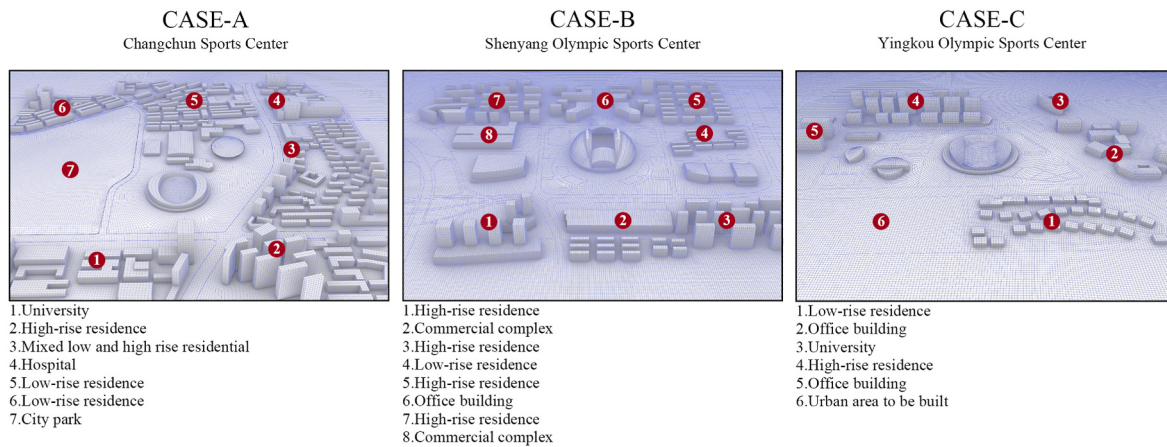


**Fig. 4.** Simulation grid diagram in computational fluid dynamics simulation.

and 1 in the winter.

Although the UTCI can be used to evaluate thermal comfort, the UTCI values of a small number of test sites do not reflect the overall thermal comfort of the site. Considering that the average thermal comfort ratio of all measuring points at the site have been used in previous studies to evaluate the thermal comfort of the use area, this study compared the average thermal comfort ratio of the site with the annual hours where overall of the site's measuring points were within the thermal comfort range ( $9^{\circ}\text{C} \leq \text{UTCI} \leq 26^{\circ}\text{C}$ ) [20]. The results illustrated that the average thermal comfort ratios of different layouts were similar, but the hours of the overall site thermal comfort of the site's measuring points within thermal comfort differed significantly in different layouts. This finding may reveal that an increase in urban thermal comfort may appear at a specific time, but not throughout the year.

### 3.3. Measurement and simulation correction

Considering the real-world situation and more accurate simulation results, the measurement results from April to May 2023 were compared with the simulation results of the same period and then adjusted and corrected through error analysis. As shown in Fig. 5(a), among the ten measurement points at each site, three measurement points with environmentally representative characteristics were selected to compare the error between the measured and simulated data. The information of the measuring equipment is shown in Table 2.

The results of the measured and simulated data analysis are shown in Fig. 5(b). When the wind speed was low, the distribution of the measured points was concentrated. When the wind speed increased, the fluctuation of the measured wind speed data increased. This may be because the building volume at the measured site was large, and the site was empty. Overall, the measured wind speed data were generally lower than the simulated data, which may have been because the effects of plants and other factors on wind speed attenuation were neglected in the simulation process. Compared with wind speed, the measured MRT data fluctuated less, and the measured average was close to the simulated value. The measured MRT data fluctuated during certain periods, which may have been due to the unstable influence of cloudy weather. A comparative analysis between the measured and simulated data shows that the degree of variation of the simulated data is basically consistent with that of the measured data. Through the fitting analysis of the measured data values and the simulated data values,  $R^2$  is greater than 0.9. This also indicates that the simulation could effectively describe the objective principles of the microclimate at these study sites.

### 3.4. Interpretation of CNN algorithm

CNN is ideal for processing image information because it can extract

complex features, classify or predict them, and has been widely explored in the field of architectural engineering [47–49]. Scholars have used the characteristics of image processing and prediction results in the field of building performance simulation [50,51]. Its basic architecture involves an input, a convolutional layer, a pooling layer, a fully connected layer, and an output. In this study, based on the Rhino-Grasshopper parameterization platform, different layout results were quickly obtained through changes in urban form index. The layout results were converted into image information. Owing to the particularity of building types such as sports centers, different requirements such as crowd evacuation, landscape, and city image must be comprehensively considered on a larger urban area scale. The complexity of the design process allows greater freedom for architects and planners. Based on the characteristics of such datasets, using a CNN to directly predict the layout performance is an effective image analysis and recognition method. At the same time, this transformation from graphics to expressions is more in line with the design logic of architects and planners. Convolutional and pooling layers were used in the CNN to extract and reduce the image features. Convolution includes a filter to extract features and an activation function (*ReLU*) to convert the sampled value into a nonlinear function [52]. According to the CNN activation function setting of existing studies on thermal comfort, *ReLU* is used in this study [53,54]. Fig. 6 illustrates the architecture of the CNN predictor used in this study.

#### 3.4.1. Image dataset

The urban form index was adjusted, and the site layouts were generated through Rhino-Grasshopper, forming 400 different layouts. As shown in Stable 2 in the Supplementary Material, RGB three-channel images with an image size of  $74 \times 144$  pixels were used as the input for the CNN. In particular, we used a grayscale map to generate a layout image of the site. The color of taller buildings with high was darker, shorter buildings were lighter, and the open space on the ground was white. The 400 layouts were simulated, and the hours of the overall site thermal comfort of the corresponding 400 sites were obtained as the output of the CNN. The two datasets were divided into a 70% training set, 15% validation set, and 15% test set.

#### 3.4.2. CNN architecture

A convolution layer takes a  $W \times H$  image patch with N-channels centered at  $x_{(i,j)}$  and two-dimensional filter-kernel  $w_f \times h_f$  as inputs, and outputs feature maps of  $(W - w_f + 1) \times (H - h_f + 1)$  with K-channels. Each channel in the output image is referred to as a filtering site. The output of the convolution process is affected by the stride  $S_f$  parameter.  $s_f$  is the distance required to slide the convolution process in an input image or feature map [55]. In this study, the CNN structure was constructed in MATLAB and consisted of three layers: the filter size was fixed to  $3 \times 3$ , the stride was 2, and zero padding was fixed to 1 to maintain the size of

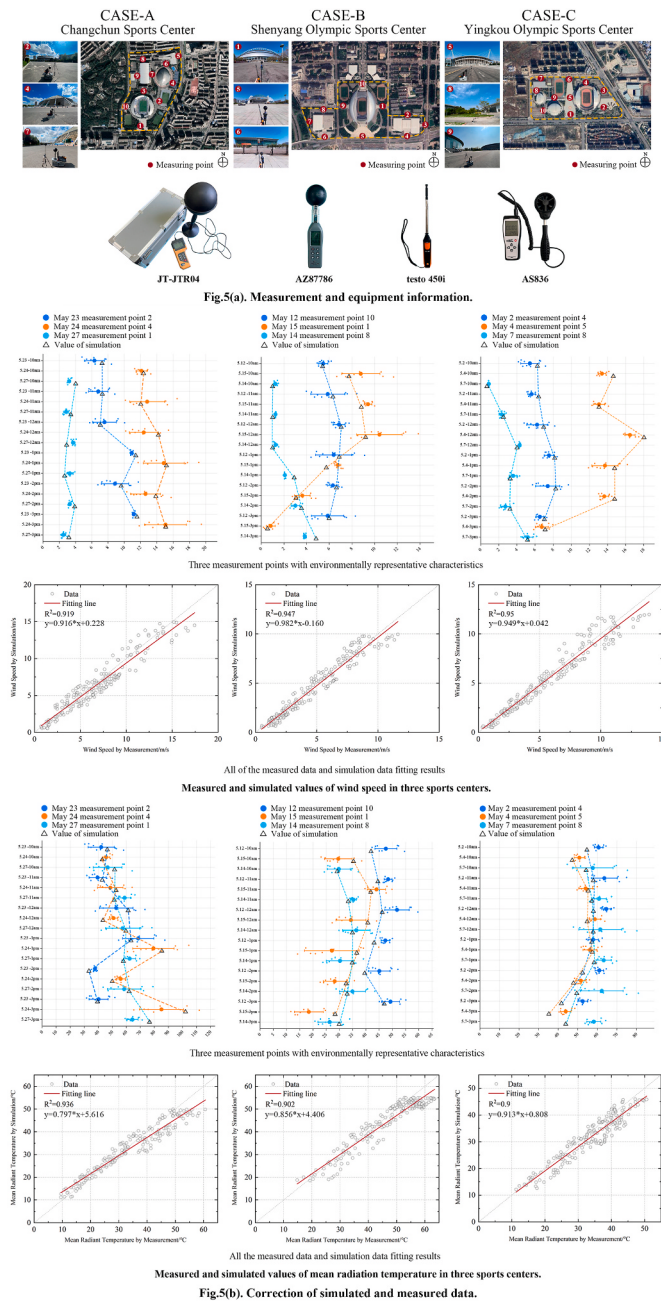


Fig. 5. Measurement and simulation correction.

**Table 2**  
Measuring equipment parameter information.

Instrument	Meteorological parameter	Measuring Range	Accuracy
JT-JTR04	Air temperature ( $T_a$ )	-20 to +85(°C)	±0.5 °C
JT-JTR04	Globe temperature ( $T_g$ , $\phi=150$ mm)	+5 to +120(°C)	±0.5 °C
AZ87786	Air temperature ( $T_a$ )	0 to +50(°C)	±0.6 °C
AZ87786	Globe temperature ( $T_g$ , $\phi=75$ mm)	0 to +80(°C)	±0.6 °C
testo 450i	Wind speed ( $V$ )	0 to 30(m/s)	±0.1 m/s
AS836	Wind speed ( $V$ )	0 to 45(m/s)	±0.2 m/s

the image. Each structure layer includes a convolution, normalization, activation function, and max pooling. The pooling layer size is  $2 \times 2$ , where the maximum value of the four pixels is input again as the pixel value in the max pooling layer. Using the 4-layer CNN structure, the

image size of  $74 \times 144$  was reduced to  $9 \times 18$  pixels. Finally, a fully connected layer fc1 with an output size of 512 and a ReLU function link dropout layer with a dropout probability of 0.09 was used. A fully connected layer fc2 with an output size of 256 and a ReLU function connected the fully connected layers for an output size of 1. The above structure is connected to the output layer for the regression task to predict the response of the trained network. During training, the mini-batch size was set to 2, the number of epochs were 20, the initial learning rate used for training was  $1e-5$ , the learning rate drop factor was 0.1, and the learning rate drop period was 20. The parameters debugging process and training results are shown in the section 4.3.1. To evaluate the performances of the CNN training results, we employed  $R^2$ , MSE and RMSE error metrics. They can be defined as [51,56]:

$$SSE = \sum_i (y_i - \hat{y}_i)^2 \quad (7)$$

$$SST = \sum_i (y_i - \bar{y})^2 \quad (8)$$

$$R^2 = 1 - SSE/SST \quad (9)$$

$$MSE = \frac{1}{n} \sum_{i=1}^n (\hat{y}_i - y_i)^2 \quad (10)$$

$$RMSE = \sqrt{\frac{1}{n} \sum_{i=1}^n (\hat{y}_i - y_i)^2} \quad (11)$$

where  $\hat{y}_i$  and  $y_i$  are the model prediction and actual output, respectively.  $\bar{y}$  is the output mean and  $n$  is the number of samples.

## 4. Results

### 4.1. Urban microclimate of sports center and surroundings

#### 4.1.1. Influence of sports center on surrounding cities

According to the above three cases, the CFD and MRT simulations and calculation of the UTCI used 5200 measuring points. Pedestrian height was selected as 1.5 m.

According to the cloud maps of the simulation results in Figs. 7–9, compared with other functional areas of the city, large sports building centers have low floor area ratios and are far from surrounding buildings, so the impact of the sports center on the surrounding urban environment is not obvious. As seen in Figs. 8 and 9, sports venues are far from the surrounding buildings, and sports buildings and venues are similar to internal regulation systems that are independent of the city. The layout of Case A in Fig. 7 is closer to the surrounding environment and has less influence. As shown in Fig. 7, at 9:00 a.m. on April 22 and 5:00 p.m. on May 16, the wind shadow area and shadow area of the venue exceeded the scope of the sports field, resulting in changes in wind speed and MRT. The wind speed was changed by 3.5 m/s, and the MRT was changed by 10.18 °C. However, compared with the significant difference in the cloud map results within the block, the impact on the thermal comfort of the surrounding city was not large.

#### 4.1.2. Influence of the surrounding city on the sports center

A low-wind-speed area is shown in the black circle in Figs. 7–9. As shown in Fig. 7, the influence was strong and the wind speed was reduced by 82.7% (4.8 m/s) until the static wind. As shown in Fig. 8, the wind speed was reduced by 20.8%–46.2% (1.2 m/s–3 m/s) compared with the surrounding area. In Fig. 9, the influence from the northwest corner of the site is relatively evident, and the wind speed was reduced by 34.2% (5 m/s) compared to the surroundings, which is related to the surrounding high-density residential buildings, high-rise residential buildings with a bottom podium, and large public buildings. As seen in the UTCI cloud chart, this can lead to poor ventilation, which in turn can

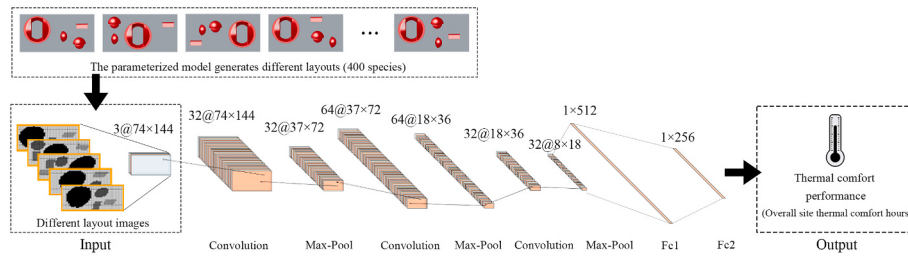


Fig. 6. Architecture of the convolutional neural network predictor.

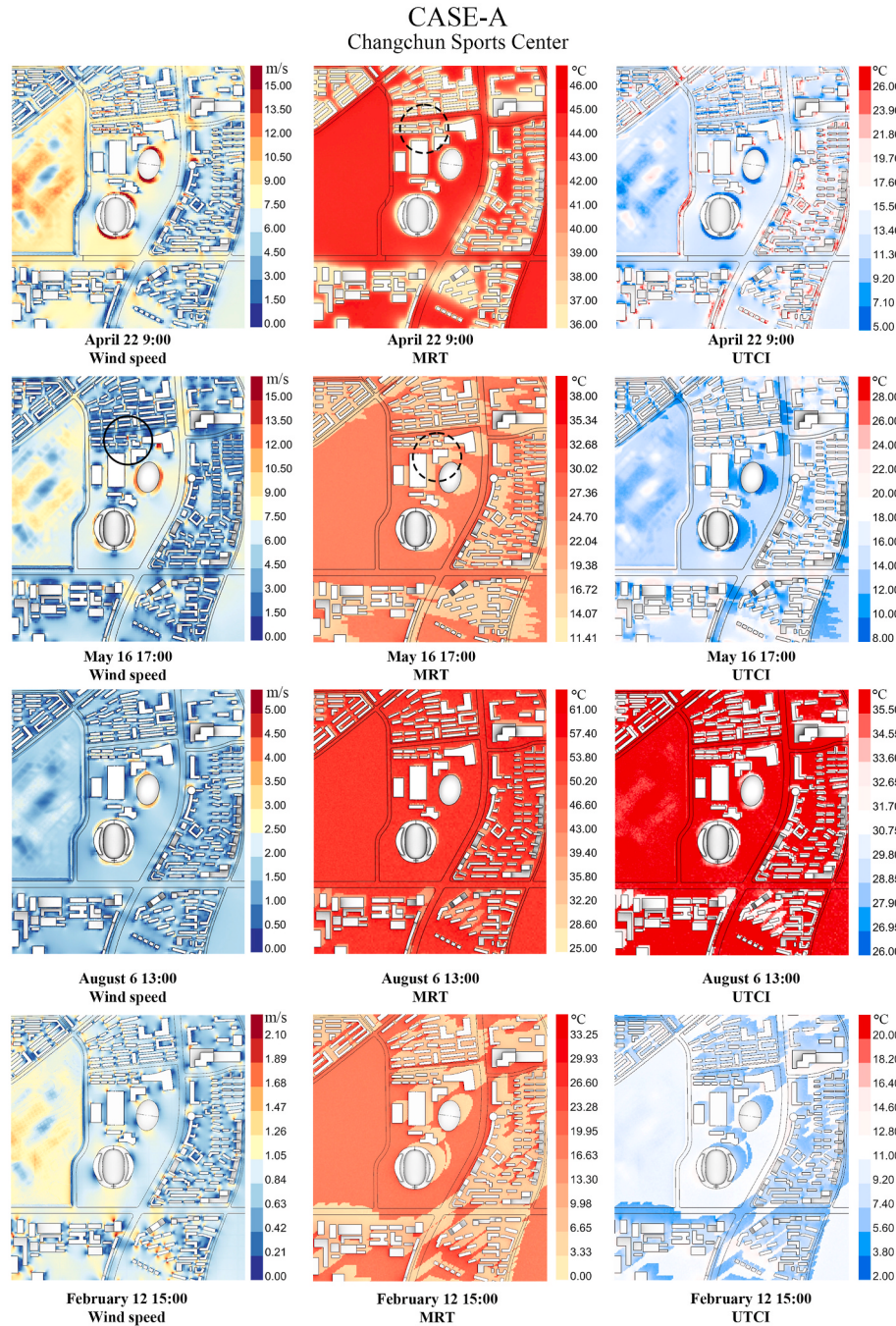
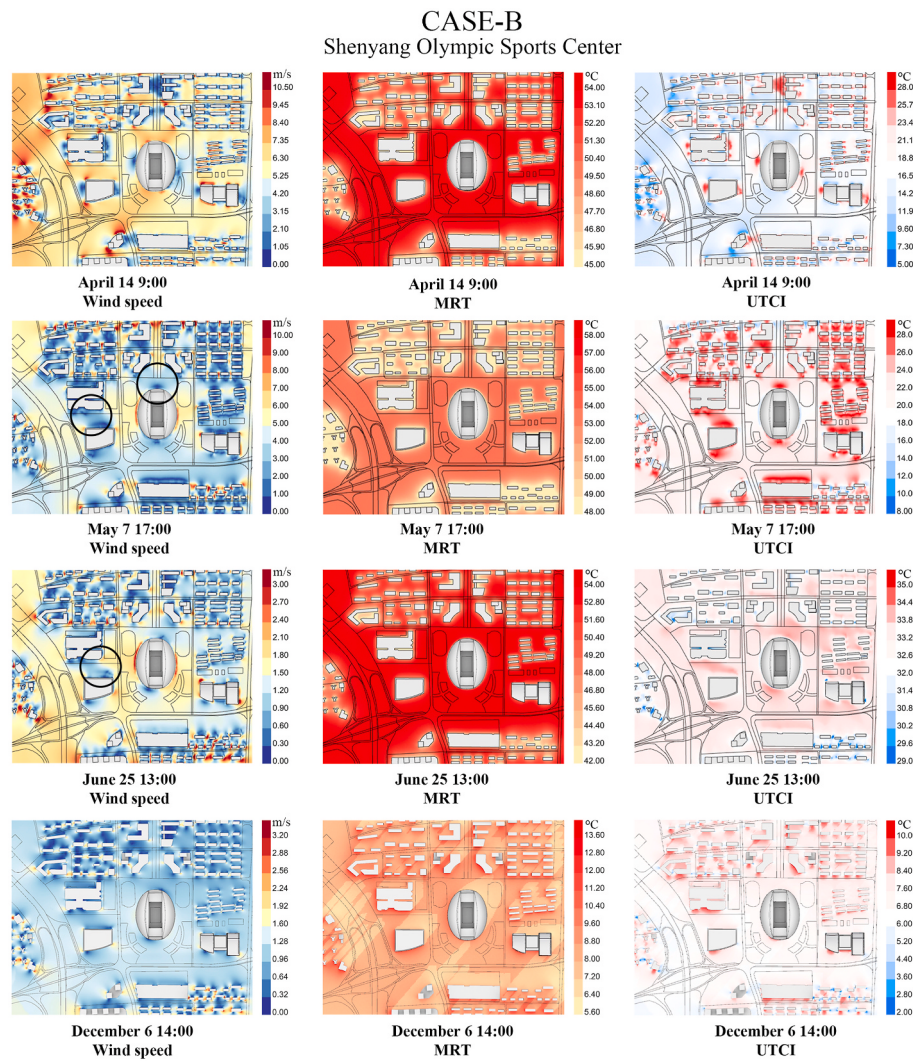


Fig. 7. Simulation cloud-chart results of Changchun Sports Center.



**Fig. 8.** Simulation cloud-chart results of Shenyang Olympic Sports Center.

lead to high temperatures, reduced thermal comfort during the hot summer months, and seasonal change periods at higher temperatures. In the study cases selected, only the shadow areas of some buildings in the black dashed circle in Fig. 7 affected the stadium of the sports center, and MRT changed by 10.7 °C. High-rise buildings and large public buildings are located far from the site, which mainly affected its wind environment. In winter, due to the occlusion of surrounding buildings, the wind speed of sites was reduced by 9%–28%. However, the large shadow area of surrounding buildings made the MRT in the shadow area (3.3 °C–13.3 °C) was greatly different from that in direct sunlight area (13.6 °C–23.4 °C).

Comparing the cloud images of the simulation results in Figs. 7–9, Fig. 7 at 5:00 p.m. on May 16, is the most typical. The UTCI cloud chart of Case A is similar to the MRT cloud chart. However, as shown in Fig. 8, at 5:00 p.m. on May 7, the UTCI cloud chart for Case B was similar to that of the wind speed cloud chart. This shows that both wind speed and MRT in the surrounding cities have obvious effects on the thermal comfort of the site; however, the importance of these effects differs for different periods. At the same time, this influence also depends on local climatic conditions. In the severely cold areas of China, the wind speed is high, which may explain why the wind environment has a relatively large impact on the thermal comfort of the site. In addition, even if a typical hour in winter with the highest insolation radiation is selected, the thermal comfort area of the site is only in the leeward low wind speed area and must not be in the shadow. This meant that, in winter, no

matter how to change the layout, the shade area of the site cannot achieve thermal comfort, and as the solar elevation angle decreases, the thermal uncomfortable area would continue to expand.

In general, the non-thermal comfort zone in addition to the high and low MRT caused by climatic factors, correlate with a surrounding urban environment with high-density residential areas with podium houses and large public buildings. This leads to poor-quality wind environments in sports centers. In the planning and layout design of these areas, the construction of indoor sports venues and reduction of the layout of outdoor activity venues should be prioritized.

#### 4.2. Influence of planning layout on thermal comfort of field area

##### 4.2.1. Influence of planning layout on wind speed and MRT

Considering that the whole site cannot achieve thermal comfort in winter in section 4.1 results, the results in section 4.2 were selected only in spring, summer and autumn. The simulation obtained annual wind speed, MRT, and UTCI data by changing the layout of two different sports centers and gyms using three urban form indices. The urban form indices are listed in Table 3. Although both wind speed and MRT have significant effects on UTCI, their degrees of influence on thermal comfort vary for different time periods. To illustrate this influence, two typical layouts compared with original layout were selected to calculate the correlation coefficient between wind speed and UTCI at 5200 measuring points on a monthly basis. The correlation coefficient

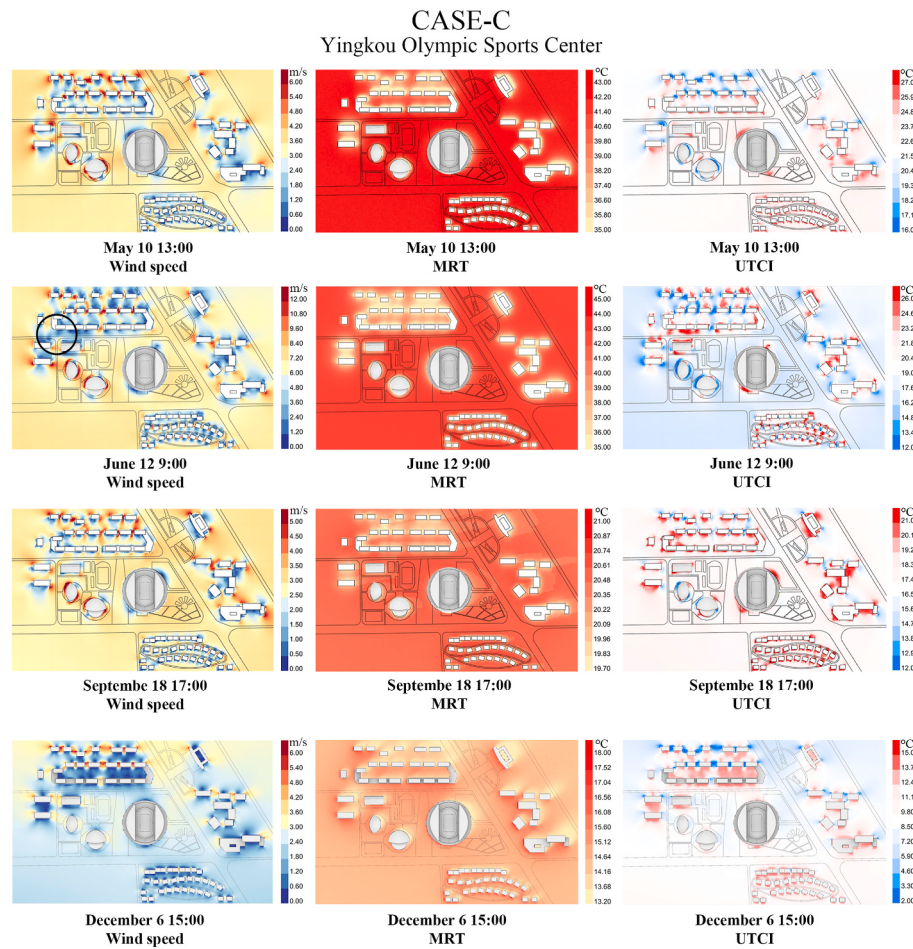


**Fig. 9.** Simulation cloud-chart results of Yingkou Olympic Sports Center.

**Table 3**  
Urban form indices of the three layouts.

Case	ESI	WFI	ALI
Original layout	2885.85	17,174.03	0.169
Case C-1	2889.80	20,255.27	0.15
Case C-2	2901.92	17,031.74	0.093

between MRT and UTCI was then calculated monthly at the same measurement point to compare the influences of wind speed and MRT on UTCI.

As shown in Fig. 10, compared with the original site layout, the change in the planned layout led to differences in the correlation

between wind speed, MRT, and UTCI; however, the overall trend was consistent. The difference in the correlation between MRT and UTCI among the three layouts was mainly reflected in March, July, August, and November. The differences in the correlation between wind speed and the UTCI were mainly reflected in May, July, August, and October. The variation in the correlation between MRT and UTCI was larger than that between wind speed and UTCI. Overall, the MRT showed a moderate positive correlation with thermal comfort in March, October, and November, and a very weak positive correlation in April. Moderately negative correlation was found for May, July, and August and a strong negative correlation was found for June and September. In contrast to the MRT, the wind speed showed a strong negative correlation from March to April, a moderate positive correlation from May to August, and

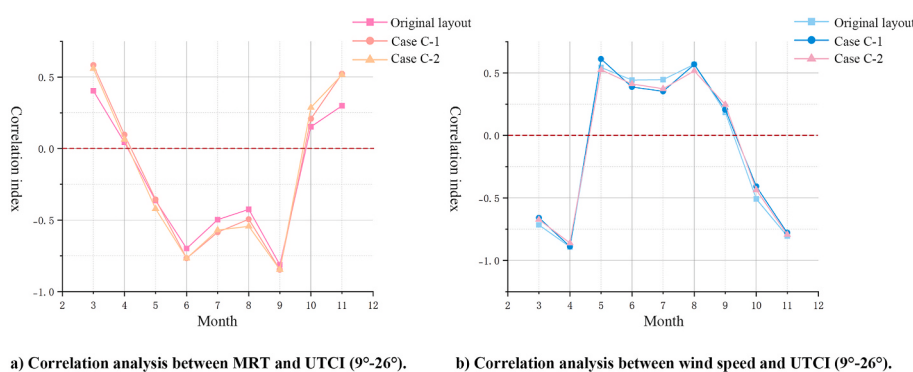


**Fig. 10.** Monthly correlation analysis of wind speed and mean radiation temperature (MRT) with universal thermal climate index (UTCI) ( $9^{\circ}\text{C}$ – $26^{\circ}\text{C}$ ).

a weak positive correlation in September. A strong negative correlation was observed between October and November. In this study, the wind speed was higher than the MRT in spring and autumn, whereas the opposite was true for summer. In August, the wind speed was similar to that during the MRT.

Among the three morphological indices, the differences between the frontal area and the intensive layout indices were relatively large. An increase in the value of the intensive layout index led to a decrease in the relevance of the MRT to thermal comfort, which may be due to the scattered building layout that expands the shadow area of the building. However, from the perspective of only three layout patterns, the amount of urban form index data is too small, and the influence is unclear and requires further analysis.

#### 4.2.2. Influence of planning layout on UTCI

As mentioned in Section 3.2, the results of the UTCI duration calculations are shown in Fig. 11. Longer periods during which the thermal comfort of overall sites of the three different layouts were concentrated in spring and autumn. Compared with the original layout, the change in duration was also concentrated in spring and autumn. From the perspective of the three layouts selected as a whole, the original layout has a thermal comfort duration of 766 h, the Case C-1 plot had a longer thermal comfort duration of 845 h, and the Case C-2 plot had the lowest thermal comfort duration of 746 h. In the current three cases, under the comprehensive influence of wind speed and MRT, the thermal comfort performance of the sports center layout in the severely cold region is mainly improved from April to June and October, especially in May, during which thermal comfort increased by a total of 26 h compared with the minimum duration. Compared with the overall duration of the minimum duration layout, the improvement rate of the maximum duration layout was 13.3%.

To explore the effects of changing the building layout on the UTCI of the site further, the outdoor activity period and sunshine conditions were considered. This study selected from 6:00 a.m. to 6:00 p.m. on April 9, June 17, and October 13. As shown in the simulation results in Fig. 12, there is a large difference between the spring and autumn seasons and a small difference in summer for the typical days of different planning layouts. The time of the thermal comfort change on April 9 was concentrated from 7:00 to 10:00 a.m. and from 3:00 to 5:00 p.m. On June 17, the heat sensation varied only slightly from 6:00 to 8:00 a.m. and from 5:00 to 6:00 p.m. On October 13, the thermal sensation changed from 7:00 to 9:00 a.m. and from 1:00 to 6:00 p.m.

The thermal sensations of the three planning layouts on April 9 ranged from moderately cold to no thermal stress, and the overall trends were essentially the same. In Case C-1, a small number of sites were in the non-thermal stress area at 6:00 a.m., accounting for 6.37%.

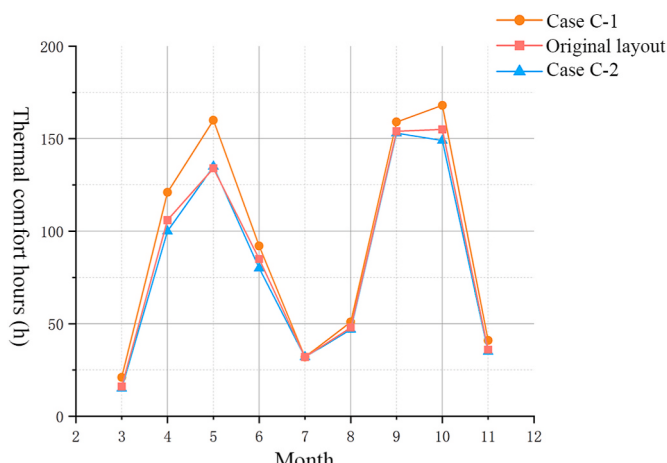


Fig. 11. Overall site thermal comfort hours by month.

However, the area with no thermal stress appeared in the original layout and Case C-2 after 7:00 a.m., and gradually expanded until 9:00 a.m. Case C-1 reached a maximum value of 100%. The original and Case C-2 layouts had a small number of slight cold stress areas accounting for 0.07% and 0.09%, respectively. However, Case C-1 and Case C-2 maintained more than 50% thermal comfort areas before 4:00 p.m., when the non-thermal stress area of the three layouts dropped sharply. The site was in a slight cold stress state at 5:00 p.m. The results were very similar, accounting for 94.48%, 90.23%, and 95.23%, respectively. On June 17, the site was in the thermal sensation zone of slight to moderate heat stress, and a small number of areas with no thermal stress appeared in the shadow area of the building. A small number of changes were mainly reflected when the daytime temperature was low from 6:00 to 7:00 a.m. and from 17:00 to 18:00 p.m. The differences between the highest and lowest proportions of slight heat stress zones at 6:00 a.m. and 6:00 p.m. were 5.74% and 7.11%, respectively. On October 13, the thermal sensation was moderately cold with no thermal stress. Thermal comfort was reached at 10:00 a.m. and began to decline after 12:00 p.m. At 2:00 p.m., the thermal comfort zones of the three site layouts decreased sharply by 24.02%, 31.37%, and 41.79%, respectively. It started to rise at 3:00 p.m. This may have been caused by wind conditions on that day. At 4:00 p.m., the percentage of the non-thermal stress areas were only 4.04%, 5.88%, and 11.51%, respectively, and the following three sites were under moderate cold stress. However, the thermal comfort zones of Case C-2 from 8:00 to 9:00 a.m. and 2:00 to 4:00 p.m. were better than the other two layouts. Taking 2:00 p.m. as an example, the nonthermal stress of the layout of Case C-2 was 17.77% higher than that of the lowest layout of Case C-1. Case C-2 outperformed the other two layouts in terms of the number of thermal comfort hours throughout the year. However, thermal conditions on a specific day do not necessarily have any advantages. When considering planning and layout design, the holding period of the event and the overall thermal comfort length of the year must be considered.

#### 4.3. CNN training results and index analysis

##### 4.3.1. Accuracy analysis of the CNN model

To derive a more general model, the model was transformed from a 3D parametric model of the building into a two-dimensional three-channel top view. In this study, the loss function was defined as the coefficient of determination ( $R^2$ ), mean square error (MSE) and root mean square error (RMSE), according to the purpose of the regression. Each model was trained 30 times to compare the optimal training results for different parameters. After changing the filter size and stride of the CNN model,  $R^2$ , MSE and RMSE are shown in the Table 4. After the above adjustment, it can be found that the training effect decreases with the increase of filter size and stride. This may be because the goal of the CNN architecture in this study is regression rather than classification, and the layout of image information is relatively simple compared to other types of images such as street view and face recognition. Therefore, the Settings in this study are the filter size selected is  $3 \times 3$  and stride is 2.

In this study, five hyperparameters of the CNN were defined: the activation function, optimization function, number of epochs, dropout factor, and mini-batch size. Table 5 summarizes the hyperparameters used in this study and their ranges. Hyperparameter tuning was performed during the dataset training. Both the convergence performance and speed of model training are considered. For the output index (overall site thermal comfort hours), the accuracy curves of the training and validation sets illustrated the process of model convergence. A training process was selected, as shown in Fig. 13, after 20 epochs of 3000 iteration. The error rate of the model tended to be low and stable. To measure the predictive performance of the model, the MSE and  $R^2$  were calculated in Fig. 14, respectively.  $R^2$  quantifies the degree of linear correlation between the predicted and measured values by calculating the accounted percentage. An  $R^2$  value close to one indicates

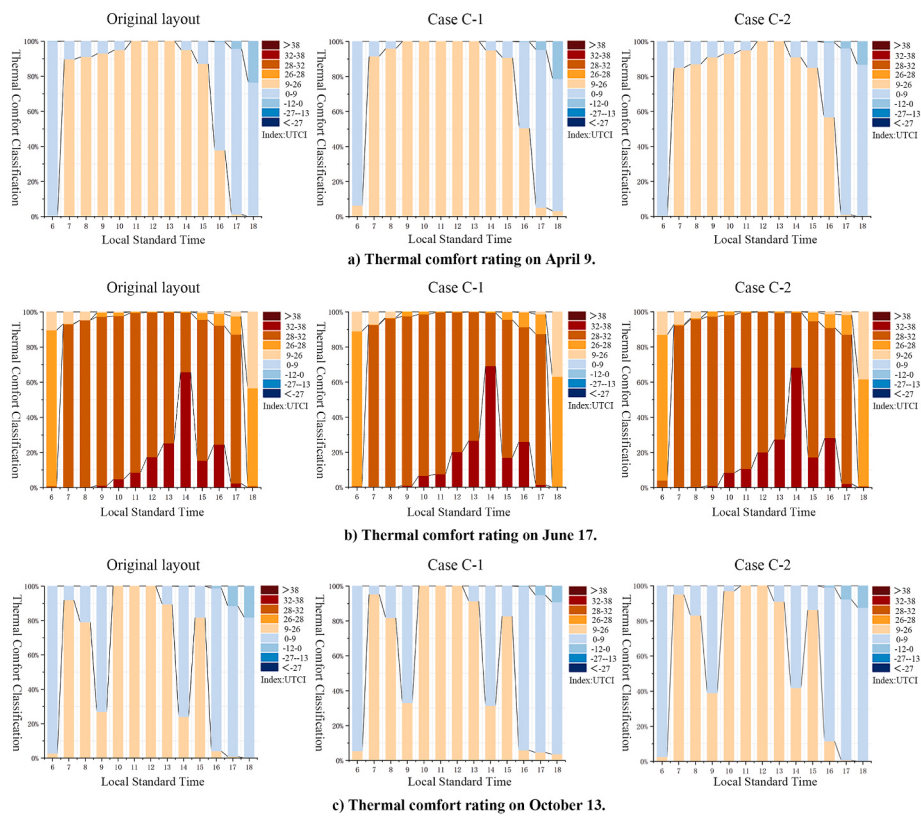


**Fig. 12.** Universal thermal climate index with different site layouts on typical days.

**Table 4**

Accuracy changes according to the choices of filter size and stride (best results reported).

Filter size	Stride	R <sup>2</sup>	MSE	RMSE
3 × 3	2	0.842	0.019	0.137
4 × 4	2	0.835	0.02	0.14
4 × 4	3	0.763	0.028	0.168
5 × 5	2	0.815	0.022	0.148
5 × 5	3	0.779	0.026	0.162
5 × 5	4	0.737	0.031	0.177
6 × 6	2	0.818	0.022	0.147
6 × 6	3	0.764	0.028	0.167
6 × 6	4	0.713	0.034	0.185
6 × 6	5	0.653	0.041	0.203

**Table 5**

Tuning range of hyperparameter for the convolutional neural network.

Hyperparameters	Range
Activation function	ReLU
Optimization function	SGDM
Number of epochs	[10, 30]
Dropout factor	[0.01, 0.1]
Mini-Batch size	[2, 32]

a high goodness of fit. MSE measures the difference between the predicted and measured values. An MSE close to zero indicates small error and high accuracy. The MSE, RMSE and R<sup>2</sup> values of the training results were 0.019, 0.137 and 0.842, respectively. Combined with the objectives of this research and considering the simulation efficiency, the proposed model has reasonable prediction performance.

#### 4.3.2. Index regression fitting and dominance range

A total of 800 sets of prediction data were obtained using the machine-learning surrogate model for the regression analysis of thermal comfort hours according to the single urban form index, as shown in Fig. 15. The R<sup>2</sup> value of the nonlinear fitting equation between the ESI and thermal comfort hours was 0.149. The R<sup>2</sup> of the nonlinear fitting equation between the WFI and thermal comfort hours was 0.137, The R<sup>2</sup> value of the nonlinear fitting equation between the ALI and thermal comfort hours was 0.225. Fig. 15 clearly shows the characteristics of urban form index and thermal comfort hours in this study. The value range of the urban form index proposed in this study was explored by considering thermal comfort hours greater than 850 h as the measurement standard. The ESI values ranged from 2876 to 2,906, the WFI ranged from 16,551 to 17,351, and the ALI ranged from 0.116 to 0.199.

According to the results, the fitting R<sup>2</sup> of the three urban form indices was not very high, which was caused by the particularity of the sports center building type and the complexity of the planning layout. The data volume may need to be further expanded. However, from the distribution of data in the figure, we can clearly determine the rule. According to this study, the ESI should not be too large or too small to balance the MRT, mainly in spring and autumn. WFI should be reduced to promote urban ventilation. The range of ALI should be appropriately increased, which may prevent the overlay of building shadow areas and promote ventilation. However, the advantage interval of this index is concentrated in the last 50% of the overall index interval, and the distribution is relatively scattered. This indicates that the distance between the stadiums and gymnasiums in the layout should not be too small. The hours of the overall site thermal comfort are relatively close after exceeding a certain threshold.

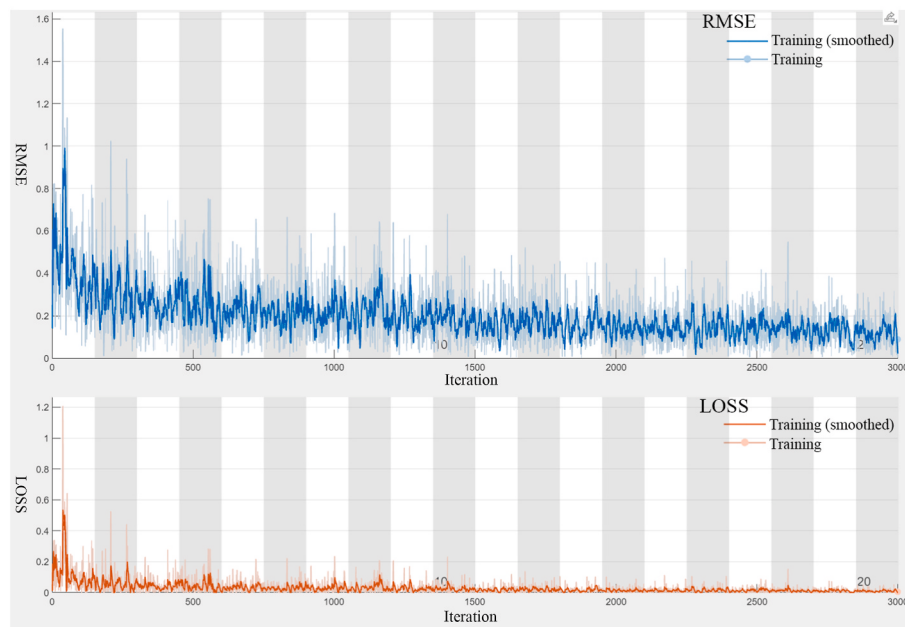


**Fig. 13.** Convolutional neural network training process.

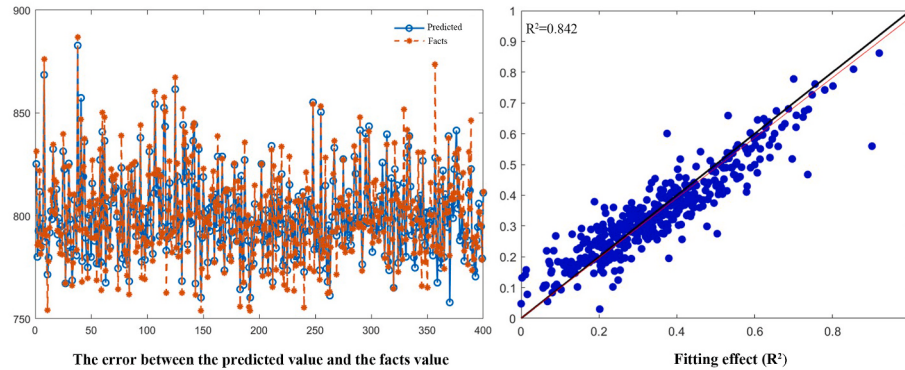


**Fig. 14.** Convolutional neural network training analysis.

## 5. Discussion

### 5.1. Reliability of simulation results

The analysis of the simulated cloud charts (Section 4.1) indicated that the thermal comfort of the outdoor activity space at the sports center site was affected by the density, height, and type of surrounding buildings, and that a greatly reduced wind speed was the main driving factor. As existing studies used the daily usage period of a typical month as the study time range [33], this study was expanded to include all activity periods of the site. However, sports events may be concentrated in a certain period, during which the use of the site will be higher than that in other periods. In future studies, it will be possible to select a high frequency of specific use periods to conduct in-depth research on the thermal comfort of sports center sites.

Although this study carried performed a month-by-month evaluation of the impact of MRT and wind speed on the thermal comfort of the outdoor spaces of sports centers in Section 4.2, the setting of the urban form around the sports center was lacking in view of the limited research case. In previous studies, the surrounding buildings were varied in terms of building height and spacing to explore the influence of the surrounding building environment on the target research site [12]. This study referred to the above methods for surrounding urban forms and

attempted to establish a semi-idealized model in order to improve the shortcomings of this study by setting different surrounding urban forms for comparison. Additionally, because the wind environment of sports center sites is affected by the surrounding building environment, the prediction performance and robustness of the method proposed in this study will be further tested.

### 5.2. Improvement of performance simulation efficiency by applying CNN

The training process and results of the CNN are presented in Section 4.3. A total of 400 sets of data were used for training and 400 sets of data were predicted using the surrogate model to analyze the influences of urban form indices on the thermal comfort of the outdoor space of the sports center. This study used 4380 h of annual use as the research period and explored the influences of different layout patterns on the thermal comfort of the site;  $400 \times 4380$  simulations were required. In some existing studies, the training sample size of the CNN was large [57, 58], and the source of the samples was photographs that were easily obtained. However, in this study, 2D images of different sports center layouts and thermal comfort performance datasets corresponding to the layouts needed to be established, which required large amounts of computing power and time. Existing studies have demonstrated the high computational cost of CFD simulations [47, 59]. Although the CNN

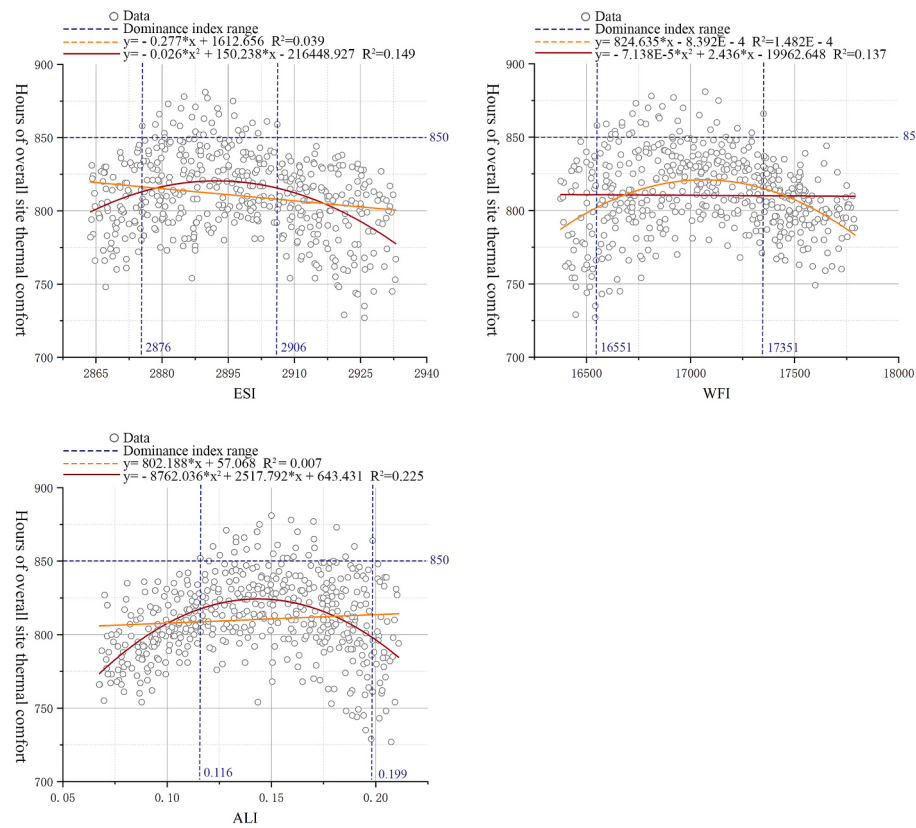


**Fig. 15.** Fitting analysis of urban form index and thermal comfort hours and the range of dominant parameters.

training results in Section 4.3.1 had MSE, RMSE, and  $R^2$  values of 0.019, 0.137, and 0.842, respectively, the error of the training results was acceptable, considering that the CNN output in this study was the number of thermal comfort hours and high calculation costs. The range of advantages of the urban form indices predicted by the simulation and surrogate models is evident and can provide a basis for early design. The application of the CNN proxy model forecasting saved considerable computational time. Studies on CNN using more than 500 training images obtained reasonable results [56]. In future work, we aim to improve the data samples trained by the CNN to obtain a more accurate surrogate model for testing the robustness of the influencing principles established in this study.

### 5.3. Practical application feasibility

This study establishes a workflow for the thermal comfort prediction of outdoor venues based on the CNN sports center layout, considering actual stadiums, gymnasiums, and the surrounding environment. In addition to improving efficiency, this method is more suitable for the actual design process during sports center construction. Owing to the importance and complexity of sports centers, various factors, such as city image and crowd evacuation, should be considered in the layout design stage. By using a CNN, designers can have more freedom to balance different factors compared with other ANNs. This is because, compared with data information, image information is more intuitive. During the early stage of design, different schemes are generated by drafting, and a trained agent model can quickly predict and compare the thermal comfort performance for a specific layout. In this study, three typical sports centers in the cold regions of China were selected to explore the influences of thermal comfort and urban microclimate. Taking Yingkou Olympic Sports Center as an example, a thermal comfort performance prediction method for the sports center layout was proposed. Although the applicability of this method is relatively high in

cold regions, considering its extensibility, thermal comfort is largely restricted by the climatic zone conditions. The prediction framework has the potential of scalability. In future studies, relevant research and verification by changing climate zones will aid in solving this problem [60].

## 6. Conclusion

Through CFD and MRT simulations, UTCI was used as an evaluation index of thermal comfort to explore the thermal comfort mechanisms in the microclimate between a sports center and the surrounding urban environment. The influence of different sports center layouts on the thermal comfort performance of the site was explored. The trained CNN performed well in predicting the thermal comfort of the different stadium layouts. Based on the simulation workflow proposed in Fig. 2, the following conclusions were drawn:

- Compared with the influence of the surrounding cities on the thermal comfort of the sports center layout and the influence of the urban form change in the surrounding block, the layout of the sports center venues had little influence on the surrounding cities; however, the lower building density of sports centers improved the ventilation of the surrounding urban area. The main influence of the surrounding cities on the layout of the sports center is on the wind environment at the site. The high-density residential buildings or large public buildings in the surrounding area led to poor ventilation of the sports center (wind speed reduced by 20.8%–82.7%) and reduced hours with overall site thermal comfort ( $9^\circ\text{C} \leq \text{UTCI} \leq 26^\circ\text{C}$ ).
- The correlation between wind speed, MRT, and UTCI of different sports center layouts from March to November changed slightly, but the overall trend was basically the same. MRT showed a positive correlation with UTCI ( $9^\circ\text{C}$ – $26^\circ\text{C}$ ) in March–April (correlation of 0.04–0.58) and October–November (correlation of 0.15–0.52), and a

- negative correlation (correlation of  $-0.36$  to  $-0.85$ ) in May–September. In contrast, the influence of the wind speed was the opposite. Wind speed showed a negative correlation with UTCI ( $9^{\circ}\text{C}$ – $26^{\circ}\text{C}$ ) in March–April (correlation of  $-0.66$  to  $-0.89$ ) and October–November (correlation of  $-0.41$  to  $-0.81$ ), and a positive correlation ( $0.18$ – $0.61$ ) in May–September. The annual difference in the hours of the overall site thermal comfort in different layouts was mainly concentrated in April–June and September–October.
3. The work framework proposed in this study is suitable for the design process of architects and planners. The trained CNN surrogate model can effectively improve the simulation efficiency. Compared with the 881 maximum hours with hours of the overall site thermal comfort of the original Yingkou Olympic Sports Center layout, the 800 different layouts simulated and predicted in this study can increase this value by 15.01%.
  4. The value range of the urban form index proposed in this study was explored by taking thermal comfort hours greater than 850 h as the measurement standard. The three urban form index advantage interval is relatively obvious. The ESI values ranged from 2876 to 2906, the WFI ranged from 16,551 to 17,351, and the ALI ranged from 0.116 to 0.199. In the future, the applicability of the three urban form indexes proposed in this paper to the evaluation of urban regional environmental performance of large-scale public building layout will be further explored.

#### CRediT authorship contribution statement

**Ao Xu:** Writing – original draft, Methodology, Conceptualization. **Yu Dong:** Writing – review & editing, Funding acquisition, Conceptualization. **Yutong Sun:** Investigation, Data curation. **Haoqi Duan:** Validation, Software, Investigation. **Ruinan Zhang:** Writing – review & editing, Validation, Supervision, Methodology, Investigation.

#### Declaration of competing interest

We declare that we have no financial and personal relationships with other people or organizations that can inappropriately influence our work, there is no professional or other personal interest of any nature or kind in any product, service or company that could be construed as influencing the position presented in the manuscript entitled.

#### Data availability

Data will be made available on request.

#### Appendix A. Supplementary data

Supplementary data to this article can be found online at <https://doi.org/10.1016/j.buildenv.2023.110917>.

#### References

- [1] S. Mirza, A. Niwalkar, S. Anjum, H. Bherwani, A. Singh, R.J.E.N. Kumar, "Studying impact of infrastructure development on urban microclimate: integrated multiparameter analysis using, Open 6 (2022), 100060.
- [2] E. Jamei, P. Rajagopalan, M. Seyedmahmoudian, Y. Jamei, Review on the impact of urban geometry and pedestrian level greening on outdoor thermal comfort, Renewable Sustainable Energy Rev. 54 (Feb 2016) 1002–1017.
- [3] J.C. Fu, Y.P. Wang, D.A. Zhou, S.J. Cao, Impact of urban park design on microclimate in cold regions using newly developed prediction method, Sustain. Cities Soc. 80 (May 2022). Art. no. 103781.
- [4] S. Yang, L.L. Wang, T. Stathopoulos, A.M.J.B. Marey, Environment, Urban Microclimate and its Impact on Built Environment-A Review, 2023, 110334.
- [5] M. Zhen, W.H. Zou, R. Zheng, Y.J. Lu, Urban outdoor thermal environment and adaptive thermal comfort during the summer, Environ. Sci. Pollut. Control Ser. 29 (51) (Nov 2022) 77864–77883.
- [6] J.A. Acero, L.A. Ruefenacht, E.J.Y. Koh, Y.S. Tan, L.K. Norford, Measuring and comparing thermal comfort in outdoor and semi-outdoor spaces in tropical Singapore, Urban Clim. 42 (Mar 2022). Art. no. 101122.
- [7] Y. Kim, S.Y. Yu, D.Y. Li, S.N. Gatson, R.D. Brown, Linking landscape spatial heterogeneity to urban heat island and outdoor human thermal comfort in Tokyo: Application of the outdoor thermal comfort index, Sustain. Cities Soc. 87 (Dec 2022). Art. no. 104262.
- [8] P. Moonen, T. Defraeye, V. Dorer, B. Blocken, J. Carmeliet, Urban physics: effect of the micro-climate on comfort, health and energy demand, Front. Architect. Res. 1 (3) (2012) 197–228.
- [9] J. Li, N. Liu, The perception, optimization strategies and prospects of outdoor thermal comfort in China: a review, Build. Environ. 170 (2020), 106614.
- [10] J. Xiao, T. Yuizon, "Climate-adaptive landscape design: microclimate and thermal comfort regulation of station square in the Hokuriku Region, Japan," in: Building and Environment, 212, Mar 15 2022, 108813.
- [11] H. Yu, H. Fukuda, M. Zhou, X. Ma, Improvement strategies for microclimate and thermal comfort for urban squares: a case of a cold climate area in China, Buildings 2 (7) (Jul 2022). Art. no. 944.
- [12] S.Y. Chan, C.K. Chau, On the study of the effects of microclimate and park and surrounding building configuration on thermal comfort in urban parks, Sustain. Cities Soc. 64 (Jan 2021), 102512.
- [13] China design code for sports building, JGJ 31 (2003).
- [14] Jun Gu, et al., China Unified Standards for Civil Building Design" GB 50352-2019, 2021, pp. 52–56.
- [15] X.D. Huang, Q.Y. Zhang, I. Tanaka, Optimization of architectural form for thermal comfort in naturally ventilated gymnasium at hot and humid climate by orthogonal experiment, Energies 14 (11) (Jun 2021). Art. no. 3228.
- [16] X.D. Huang, X.L. Ma, Q.Y. Zhang, Effect of building interface form on thermal comfort in gymnasiums in hot and humid climates, Frontiers of Architectural Research 8 (1) (Mar 2019) 32–43.
- [17] Y.F. Bai, L.T. Zhao, R.N. Tang, X.L. Kang, Study on winter thermal comfort of membrane structure gymnasium in severe cold region of China, Science and Technology for the Built Environment 28 (4) (May 2022) 499–512.
- [18] G. Losi, A. Bonzanini, A. Aquino, P. Poesio, Analysis of thermal comfort in a football stadium designed for hot and humid climates by CFD, J. Build. Eng. 33 (Jan 2021). Art. no. 101599.
- [19] S. Ghani, A.O. Mahgoub, F. Bakochristou, E.A. ElBialy, Assessment of thermal comfort indices in an open air-conditioned stadium in hot and arid environment, J. Build. Eng. 40 (Aug 2021). Art. no. 102378.
- [20] R. Zhang, D. Liu, L. Shi, Thermal-comfort optimization design method for semi-outdoor stadium using machine learning, Build. Environ. 215 (May 1 2022). Art. no. 108890.
- [21] H.-U. Kim, S.-I. Jong, Development of a system for evaluating the flow field around a massive stadium: combining a microclimate model and a CFD model, Build. Environ. 172 (Apr 2020). Art. no. 106736.
- [22] J.Y. Deng, N.H. Wong, Impact of urban canyon geometries on outdoor thermal comfort in central business districts, Sustain. Cities Soc. 53 (Feb 2020). Art. no. 101966.
- [23] J. Graham, U. Berardi, G. Turnbull, R. McKaye, Microclimate analysis as a design driver of architecture, Climate 8 (6) (Jun 2020). Art. no. 72.
- [24] L. Chen, E. Ng, Outdoor thermal comfort and outdoor activities: a review of research in the past decade, Cities 29 (2) (Apr 2012) 118–125.
- [25] R. Aghamolaei, M. M. Azizi, B. Aminzadeh, and J. O'Donnell, "A Comprehensive Review of Outdoor Thermal Comfort in Urban Areas: Effective Parameters and Approaches," Energy & Environment.
- [26] E.S. Darbani, D.M. Parapari, J. Boland, E. Sharifi, Impacts of urban form and urban heat island on the outdoor thermal comfort: a pilot study on Mashhad, Int. J. Biometeorol. 65 (7) (Jul 2021) 1101–1117.
- [27] J.L. Zhang, Z. Li, Y.X. Wei, D. Hu, The impact of the building morphology on microclimate and thermal comfort-a case study in Beijing, Build. Environ. 223 (Sep 2022). Art. no. 109469.
- [28] X.Z. Zhang, et al., Estimating the outdoor environment of workers' villages in East China using machine learning, Build. Environ. 226 (Dec 2022). Art. no. 109738.
- [29] X. He, W. Gao, R. Wang, Impact of urban morphology on the microclimate around elementary schools: a case study from Japan, Build. Environ. 206 (Dec 2021). Art. no. 108383.
- [30] O.M. Galal, D.J. Sailor, H. Mahmoud, The impact of urban form on outdoor thermal comfort in hot arid environments during daylight hours, case study: new Aswan, Build. Environ. 184 (Oct 2020). Art. no. 107222.
- [31] G. Jang, S. Kim, J.S. Lee, Planning scenarios and microclimatic effects: the case of high-density riverside residential districts in Seoul, South Korea, Build. Environ. 223 (Sep 2022). Art. no. 109517.
- [32] N. Eslamirad, F.D. Luca, K.S. Lylykangas, S.B. Yahia, Data Generative Machine Learning Model for the Assessment of Outdoor Thermal and Wind Comfort in a Northern Urban Environment, Front. Architect. Res. 12 (3) (2023) 541–555.
- [33] R. Sun, J. Liu, D. Lai, W. Liu, Building form and outdoor thermal comfort: inverse design the microclimate of outdoor space for a kindergarten, Energy Build. 284 (2023/04/01/2023), 112824.
- [34] C. Sun, W.Y. Lian, L. Liu, Q. Dong, Y.S. Han, The impact of street geometry on outdoor thermal comfort within three different urban forms in severe cold region of China, Build. Environ. 222 (Aug 2022). Art. no. 109342.
- [35] J.-Y. Deng, Y. He, M.J.B. Dai, Environment, Evaluation of the Outdoor Thermal Environment for Three Typical Urban Forms in Nanjing, 2023, 110358. China.
- [36] M. Hajdukiewicz, M. Geron, M.M. Keane, Formal calibration methodology for CFD models of naturally ventilated indoor environments, Build. Environ. 59 (Jan 2013) 290–302.
- [37] L. Wang, N.H. Wong, Coupled simulations for naturally ventilated residential buildings, Autom. ConStruct. 17 (4) (May 2008) 386–398.

- [38] M. Heidarinejad, et al., Influence of building surface solar irradiance on environmental temperatures in urban neighborhoods, *Sustain. Cities Soc.* 26 (Oct 2016) 186–202.
- [39] Y.K. Yi, N. Feng, Dynamic integration between building energy simulation (BES) and computational fluid dynamics (CFD) simulation for building exterior surface, *Build. Simulat.* 6 (3) (Sep 2013) 297–308.
- [40] Y. Li, Y.K. Yi, Optimal Shape Design Using Machine Learning for Wind Energy and Pressure, *J.O.B.E.* 70 (2023), 106337.
- [41] F. Ding, A.J.E. Kareem, Tall buildings with dynamic facade under winds 6 (12) (2020) 1443–1453.
- [42] F.R.D. Alfano, M. Dell'Isola, B.I. Palella, G. Riccio, A. Russi, On the measurement of the mean radiant temperature and its influence on the indoor thermal environment assessment, *Build. Environ.* 63 (May 2013) 79–88.
- [43] H. Guo, D. Aviv, M. Loyola, E. Teitelbaum, N. Houchois, F. Meggers, On the understanding of the mean radiant temperature within both the indoor and outdoor environment, a critical review, *Renewable Sustainable Energy Rev.* 117 (Jan 2020). Art. no. 109207.
- [44] Z. Fang, Z. Zheng, X. Feng, D. Shi, Z. Lin, Y. Gao, Investigation of outdoor thermal comfort prediction models in South China: a case study in Guangzhou, *Build. Environ.* 188 (Jan 15 2021). Art. no. 107424.
- [45] B. Wang, Y.K. Yi, Developing an Adapted UTCI (Universal Thermal Climate Index) for the Elderly Population in China's Severe Cold Climate Region 69, *Sustainable Cities and Society*, Jun 2021. Art. no. 102813.
- [46] J. Li, J. Niu, C.M. Mak, T. Huang, Y. Xie, Exploration of applicability of UTCI and thermally comfortable sun and wind conditions outdoors in a subtropical city of Hong Kong, *Sustain. Cities Soc.* 52 (Jan 2020). Art. no. 101793.
- [47] G. Calzolari, W. Liu, Deep learning to replace, improve, or aid CFD analysis in built environment applications: a review, *Build. Environ.* 206 (Dec 2021). Art. no. 108315.
- [48] J. Baek, D.Y. Park, H. Park, D.M. Le, S. Chang, Vision-based personal thermal comfort prediction based on half-body thermal distribution, *Build. Environ.* 228 (Jan 15 2023). Art. no. 109877.
- [49] C. Sun, X. Guo, T. Zhao, Y. Han, Real-time detection method of window opening behavior using deep learning-based image recognition in severe cold regions, *Energy Build.* 268 (Aug 1 2022). Art. no. 112196.
- [50] P. Liu, et al., Towards Human-Centric Digital Twins: Leveraging Computer Vision and Graph Models to Predict Outdoor Comfort 93, *Sustainable Cities and Society*, Jun 2023. Art. no. 104480.
- [51] F. Elmaz, R. Eyckerman, W. Casteels, S. Latre, P. Hellinckx, CNN-LSTM architecture for predictive indoor temperature modeling, *Build. Environ.* 206 (Dec 2021). Art. no. 108327.
- [52] Z. Li, F. Liu, W. Yang, S. Peng, J. Zhou, A survey of convolutional neural networks: analysis, applications, and prospects, *IEEE Transact. Neural Networks Learn. Syst.* 33 (12) (Dec 2022) 6999–7019.
- [53] F. Briegel, O. Makansi, T. Brox, A. Matzarakis, A.J.U.C. Christen, "Modelling Long-Term Thermal Comfort Conditions in Urban Environments Using a Deep Convolutional Encoder-Decoder as a Computational Shortcut," 47, 2023, 101359.
- [54] N. Somu, A. Sriram, A. Kowli, K.J.B. Ramamritham, Environment, A Hybrid Deep Transfer Learning Strategy for Thermal Comfort Prediction in Buildings, 204, 2021, 108133.
- [55] R.F. Nogueira, R. de Alencar Lotufo, R.C. Machado, Fingerprint liveness detection using convolutional neural networks, *IEEE transactions on information forensics and security* 11 (6) (2016) 1206–1213.
- [56] Q. He, et al., Predictive Models for Daylight Performance of General Floorplans Based on CNN and GAN: a Proof-Of-Concept Study, 206, 2021, 108346.
- [57] Z. Wang, et al., "Quantifying legibility of indoor spaces using deep convolutional neural networks, Case studies in train stations," 160 (2019), 106099.
- [58] S. Hu, J. Sun, J. Zhang, G. Liu, S.J.B. Zhao, Environment, Thermoacoustic Environment Comfort Evaluation Method Based on Facial Micro-expression Recognition, 221, 2022, 109263.
- [59] S. Xiang, et al., Fast Simulation of High Resolution Urban Wind Fields at City Scale, 39, 2021, 100941.
- [60] S. Mirzabeigi, M.J.S.C. Razkenari, Society, Design Optimization of Urban Typologies: A Framework for Evaluating Building Energy Performance and Outdoor Thermal Comfort, 76, 2022, 103515.